

MIT Open Access Articles

Thalamocortical synchronization during induction and emergence from propofol-induced unconsciousness

The MIT Faculty has made this article openly available. **Please share** how this access benefits you. Your story matters.

Citation: Flores, Francisco J. et al. "Thalamocortical Synchronization During Induction and Emergence from Propofol-Induced Unconsciousness." *Proceedings of the National Academy of Sciences* 114, 32 (July 2017): E6660–E6668 © 2017 National Academy of Sciences

As Published: <http://dx.doi.org/10.1073/PNAS.1700148114>

Publisher: National Academy of Sciences (U.S.)

Persistent URL: <http://hdl.handle.net/1721.1/113858>

Version: Final published version: final published article, as it appeared in a journal, conference proceedings, or other formally published context

Terms of Use: Article is made available in accordance with the publisher's policy and may be subject to US copyright law. Please refer to the publisher's site for terms of use.



Thalamocortical synchronization during induction and emergence from propofol-induced unconsciousness

Francisco J. Flores^{a,b,c,1}, Katharine E. Hartnack^a, Amanda B. Fath^{d,e}, Seong-Eun Kim^{c,2}, Matthew A. Wilson^{c,e}, Emery N. Brown^{a,b,c,e,f,1,3}, and Patrick L. Purdon^{a,b,1,3}

^aDepartment of Anesthesia, Critical Care, and Pain Medicine, Massachusetts General Hospital, Boston, MA 02114; ^bHarvard Medical School, Boston, MA 02115; ^cPicower Institute for Learning and Memory, Massachusetts Institute of Technology, Cambridge, MA 02139; ^dDepartment of Neuroscience, Wellesley College, Wellesley, MA 02481; ^eDepartment of Brain and Cognitive Sciences, Massachusetts Institute of Technology, Cambridge, MA 02139; and ^fInstitute of Medical Engineering and Sciences, Massachusetts Institute of Technology, Cambridge, MA 02139

Edited by Terrence J. Sejnowski, Salk Institute for Biological Studies, La Jolla, CA, and approved June 21, 2017 (received for review January 25, 2017)

General anesthesia (GA) is a reversible drug-induced state of altered arousal required for more than 60,000 surgical procedures each day in the United States alone. Sedation and unconsciousness under GA are associated with stereotyped electrophysiological oscillations that are thought to reflect profound disruptions of activity in neuronal circuits that mediate awareness and cognition. Computational models make specific predictions about the role of the cortex and thalamus in these oscillations. In this paper, we provide in vivo evidence in rats that alpha oscillations (10–15 Hz) induced by the commonly used anesthetic drug propofol are synchronized between the thalamus and the medial prefrontal cortex. We also show that at deep levels of unconsciousness where movement ceases, coherent thalamocortical delta oscillations (1–5 Hz) develop, distinct from concurrent slow oscillations (0.1–1 Hz). The structure of these oscillations in both cortex and thalamus closely parallel those observed in the human electroencephalogram during propofol-induced unconsciousness. During emergence from GA, this synchronized activity dissipates in a sequence different from that observed during loss of consciousness. A possible explanation is that recovery from anesthesia-induced unconsciousness follows a “boot-up” sequence actively driven by ascending arousal centers. The involvement of medial prefrontal cortex suggests that when these oscillations (alpha, delta, slow) are observed in humans, self-awareness and internal consciousness would be impaired if not abolished. These studies advance our understanding of anesthesia-induced unconsciousness and altered arousal and further establish principled neurophysiological markers of these states.

anesthesia | prefrontal cortex | thalamus | coherence | propofol

General anesthesia (GA) is a reversible drug-induced state consisting of unconsciousness, analgesia, amnesia, akinesia, and physiological stability (1). In the United States nearly 60,000 surgical procedures are conducted under GA every day, making GA one of the most common manipulations of the brain and central nervous system in medicine (1). The molecular mechanisms by which anesthetic drugs alter brain function have been well characterized (2, 3). Detailed analyses of neural circuit- and systems-level mechanisms of GA are more recent (1, 4, 5). Understanding the system-wide effects of anesthetic drugs is necessary in order to understand how these drugs produce states of altered arousal and unconsciousness.

One of the most commonly used anesthetic drugs is 2,6-diisopropylphenol (propofol), a GABA-A receptor agonist (6). Electroencephalogram (EEG) recordings in humans during gradual induction of unconsciousness with propofol show the appearance of frontal β oscillations (15–30 Hz) at the onset of sedation, followed by the appearance of coherent frontal α (8–12 Hz) oscillations (7–10) and widespread slow (0.1–1 Hz) and δ (1–4 Hz) oscillations (7, 11, 12) when subjects no longer respond to sensory stimuli. Biophysical models of neuronal dynamics have shown that whereas α and β oscillations can be generated by propofol's actions in cortex alone (13), coherent α

oscillations require the participation of both thalamus and cortex (14). Imaging studies in humans have shown that propofol disrupts functional relationships between cortex and thalamus, eliciting a greater degree of disruption between cortex and higher-order thalamic nuclei compared with first-order nuclei (15). Together, these results suggest that propofol could produce states of altered arousal and unconsciousness in part by disrupting activity within the thalamocortical system. In particular, they support the hypothesis that loss of consciousness would correlate with the development of coherent α oscillations engaging thalamus and cortex, whereas recovery of consciousness would correlate with the dissipation of these coherent oscillations.

To test these hypotheses, we implanted Sprague-Dawley rats with electrodes in different layers of medial prefrontal (prelimbic) cortex and in different higher-order thalamic nuclei. We recorded field potentials during gradual induction of unconsciousness using propofol and during passive emergence from unconsciousness. We found that the rodent frontal cortical local field potential (LFP) reproduces the sequence of EEG oscillations observed in humans during propofol-induced anesthesia.

Significance

General anesthesia is a drug-induced state of altered arousal associated with profound, stereotyped electrophysiological oscillations. Here we report evidence in rats that propofol, an anesthetic drug frequently used in clinical practice, disrupts activity in medial prefrontal cortex and thalamus by inducing highly synchronized oscillations between these structures. These oscillations closely parallel human electroencephalogram oscillations under propofol. Disruption of activity in medial prefrontal cortex by these oscillations implies an impairment of self-awareness and internal consciousness. During recovery of consciousness, these synchronized oscillations dissipate in a “boot-up” sequence most likely driven by ascending arousal centers. These studies advance our understanding of what it means to be unconscious under anesthesia and establish principled neurophysiological markers to monitor and manage this state.

Author contributions: F.J.F., M.A.W., E.N.B., and P.L.P. designed research; F.J.F., K.E.H., and A.B.F. performed research; F.J.F., K.E.H., A.B.F., S.-E.K., M.A.W., E.N.B., and P.L.P. analyzed data; and F.J.F. and P.L.P. wrote the paper.

Conflict of interest statement: E.N.B. and P.L.P. have patents pending on anesthesia monitoring.

This article is a PNAS Direct Submission.

Freely available online through the PNAS open access option.

¹To whom correspondence may be addressed. Email: patrickp@nmr.mgh.harvard.edu, ffflores@neurostat.mit.edu, or enb@neurostat.mit.edu.

²Present address: Department of Electronics and Control Engineering, Hanbat National University, Daejeon 305-719, Korea.

³E.N.B. and P.L.P. contributed equally to this work.

This article contains supporting information online at www.pnas.org/lookup/suppl/doi:10.1073/pnas.1700148114/-DCSupplemental.

Propofol-induced α oscillations that develop at loss of consciousness, measured behaviorally by loss of righting reflex, are highly coherent between higher-order thalamus and prefrontal cortex. Soon after, α and slow- δ oscillations develop at the point of complete loss of movement, which also display high thalamocortical coherence at α and δ frequencies. During emergence, the δ oscillations diminish in power and are no longer thalamocortically coherent before recovery of movement. In the α range, midline thalamic nuclei and deep prefrontal layers are no longer coherent, implying that parts of the thalamocortical system can become functional before others during emergence.

Results

Overview. We recorded LFPs in prefrontal cortex and thalamus during the gradual transition from an awake, freely behaving state through loss of righting reflex and movement induced by a slowly increasing infusion rate of propofol (*Materials and Methods* and Fig. S1). We then allowed the animals to passively recover from the anesthetic. Throughout the experiment, we characterized the movement and behavior of the animals, using video recordings. We performed a total of 11 experiments in eight rats. We identified the time of loss of righting reflex (LORR), loss of movement (LOM), recovery of movement (ROM), and recovery of righting reflex (RORR) as the relevant behavioral endpoints to analyze the electrophysiological dynamics (SI Results and Fig. S2).

Electrophysiological Dynamics of Rodent Prefrontal Cortex Parallel the Human EEG During Induction of and Emergence from Anesthesia. In humans, a well-defined pattern of oscillations has been observed during transition into propofol-induced unconsciousness. This pattern includes β oscillations that smoothly transition into α oscillations at the time of loss of consciousness (7, 8). EEG source localization analyses in humans suggest that these β and α oscillations are generated approximately within dorsal medial prefrontal and anterior cingulate cortices (16). We therefore investigated whether LFP activity in the rodent medial prefrontal cortex, which is thought to correspond to the human dorsal medial prefrontal and anterior cingulate cortices (17), would show a pattern of oscillations under propofol similar to that in humans. To investigate this question, we computed time-varying spectra (spectrograms) (18) to analyze the dynamics of the LFP oscillations. We extracted the portion of the spectrograms around or after the different behavioral events and aggregated them across recording sites and animals, to obtain group peri-event spectra, which we subsequently analyzed for statistical significance (*Materials and Methods*).

During baseline, the raw LFP trace displayed low amplitude with no obvious oscillations, typical of the awake state (Fig. 1A). The group spectra ($n = 27$, eight rats) showed decay in power from lower to higher frequencies (19) (Fig. 1B). During induction of anesthesia, the nonnormalized (Fig. 1C) and baseline-normalized (Fig. 1D) spectrograms showed the appearance of β oscillations (15–30 Hz) soon after dosing started, which transitioned to α oscillations (10–15 Hz), at which time LORR occurred, and subsequently to simultaneous slow (0.1–1 Hz), δ (1–5 Hz), and α oscillations, at which time LOM occurred. Focusing on the period that precedes LORR (preLORR), the β oscillations can be observed in the raw trace (Fig. 1E, blue trace). The difference group spectra revealed a significant increase at all frequencies except the slow and θ bands (Fig. 1F). The β band had a peak at a frequency (f_p) of 26 Hz and showed a significant power increase. Another significant power increase can be observed in the δ band ($f_p = 3.6$ Hz) (Fig. 1D and F and Table 1).

As the infusion continued, power significantly increased at most frequencies except for the slow band. Focusing on the LORR period, we observed that the raw trace displays a semi-

continuous α oscillation (Fig. 1E, green trace). The group difference spectra showed significant power increase in the δ ($f_p = 4.3$ Hz) and α bands ($f_p = 12.20$ Hz) (Fig. 1F and Table 1). After LORR occurred, the animals continued to perform nonpurposeful head and/or limb movements. Focusing on the LOM period, we observed a further increase in the amplitude of slow, δ and α oscillations (Fig. 1C, Left, red trace). The group difference spectra revealed a significant increase in power at all frequency bands, but with clear peaks in the δ ($f_p = 4.3$ Hz) and α ($f_p = 12.2$ Hz) bands (Fig. 1D and F and Table 1).

The oscillatory features observed during emergence differed from those observed during induction in some of their features. The nonnormalized (Fig. 1G) and baseline-normalized (Fig. 1H) spectrograms showed the presence of slow, δ , and α oscillations previous to ROM. Right after ROM, a sudden change to β oscillations occurred, which decrease in power after RORR (Fig. 1H). Focusing on the period before ROM (preROM), the raw traces showed the slow, δ , and α oscillations (Fig. 1D, blue trace). We observed that the group difference spectra is still significantly higher than baseline at all frequencies, but displayed spectral peaks at δ ($f_p = 4.2$ Hz) and α ($f_p = 11$ Hz) (Fig. 1J and Table 1). Focusing on the period after ROM, the difference group spectra showed a power increase only beyond the θ band (Fig. 1J), with a significant peak only in the β band ($f_p = 19.3$ Hz; Table 1). After RORR, the difference group spectra were very similar to those observed during ROM, with peaks in the δ ($f_p = 4.4$ Hz) and β bands ($f_p = 23.3$ Hz; Fig. 1J and Table 1). Thus, on emergence, the electrophysiological dynamics appeared to change abruptly at ROM from α , slow, and δ oscillations to β oscillations, distinct from the more gradual transition that we observed during induction.

Layers of Prefrontal Cortex Are Differentially Affected by Propofol Actions. Different cortical layers in prefrontal cortex display different connectivity patterns with thalamus and other cortical and subcortical areas. Also, the model put forward by Ching et al. (14) assumed a generic prefrontal layer 5 neuron. Therefore, we investigated the possibility of different layers being differentially affected by propofol. We estimated the electrode locations as described in *Materials and Methods* (layer 2/3, $n = 8$, five rats; layer 5, $n = 12$, seven rats; layer 6, $n = 7$, four rats). Example raw LFPs recorded after LORR showed a subtle but visible increase in the amplitude of the traces going from superficial layer 2/3 to the deeper layers 5 and 6 (Fig. 2A, yellow highlight). When we analyzed the power difference between all pairs of layers (Fig. 2B), no differences in power were observed during the preLORR state, but at LORR, layers 5 and 6 showed significantly higher power than layer 2/3 in the α band (5 vs. 2/3, $f_p = 13.6$ Hz; 6 vs. 2/3, $f_p = 13.5$ Hz) (Fig. 2B and Table S1). During the LOM period, the difference in power at α disappeared, but layers 5 and 6 showed higher power than layer 2/3 in the slow (5 vs. 2/3, $f_p = 0.8$ Hz; 6 vs. 2/3, $f_p = 0.4$ Hz) and δ ranges (5 vs. 2/3, $f_p = 3.44$ Hz; 6 vs. 2/3, $f_p = 3.6$ Hz) (Fig. 2B and Table S1).

During emergence, the differential effects of propofol in the superficial (2/3) and deep layers (5 and 6) are still present. Example raw LFP traces corresponding to the preROM period show the trend to higher amplitude in deeper layers (Fig. 2C, yellow highlight). When we analyzed the power difference between all pairs of layers (Fig. 2D), we found that in the preROM period, power in layer 6 was significantly greater than power in both layers 2/3 and 5, in the slow (6 vs. 2/3, $f_p = 0.1$ Hz; 6 vs. 5, $f_p = 0.7$ Hz) and δ ranges (6 vs. 2/3, $f_p = 1.2$ Hz; 6 vs. 5, $f_p = 1.2$ Hz) (Fig. 2D and Table S1). Immediately after ROM, all differences in power disappeared, and during RORR, the power in layer 6 became significantly lower than power in both layers 2/3 and 5 in the δ range (6 vs. 2/3, $f_p = 2.8$ Hz dB; 6 vs. 5, $f_p = 1.2$ Hz), and power in layer 6 was also significantly lower than in layer 2/3 in

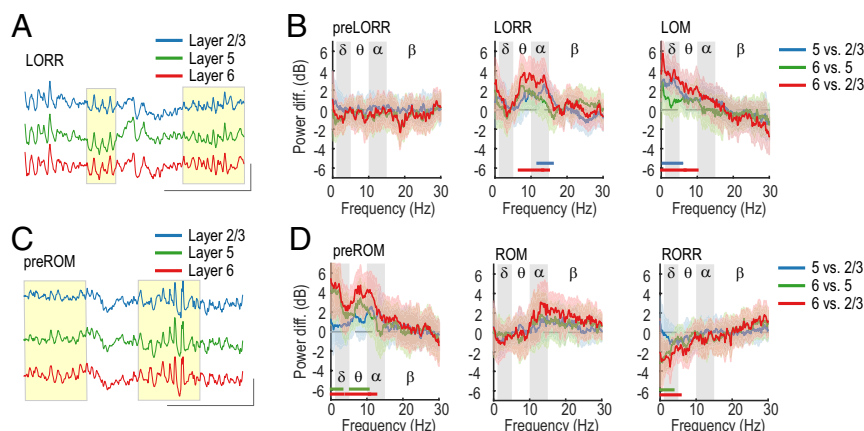


Fig. 2. Differential effects of propofol in deep and superficial layers. (A and B) Difference in power between layers during induction of anesthesia. (A) Example raw traces observed during LORR from electrodes located in layers 2/3 (blue), 5 (green), and 6 (red). (B) Baseline-normalized, difference group spectra between layers, at each behavioral event. Shaded area represents 99% confidence intervals. (C and D) Difference in power between layers during emergence from anesthesia. (C) Example raw traces observed during preROM from electrodes located in layers 2/3, 5, and 6. Color code is the same as in A. (D) Baseline-normalized, difference group spectra at each behavioral event. Color code is the same as in B. In A and C, the yellow squares highlight portions of the raw traces where deep layers display bigger amplitude than superficial layers. The shaded area in all group spectra represents 99% confidence intervals, and the horizontal lines mark the frequencies at which power is significantly different from baseline beyond the spectral resolution (3 Hz). Vertical scale: 1,000 μ V. Horizontal scale: 1 s.

origin (20). Example spectrograms show the full sequence of changes observed after the start of propofol dosing (Fig. 3 C and D). Before LORR, the thalamic spectrogram displayed increased power in the β and δ bands, which can be seen more clearly in the baseline-normalized spectrogram (Fig. 3D) and can also be observed in the raw trace (Fig. 3E). The difference group spectrum, computed 3 min preLORR, showed that the β oscillation is significantly higher than baseline, peaking at $f_p = 26.3$ Hz. The group spectrum also revealed a second significant peak spanning the slow and δ bands ($f_p = 3.7$ Hz) (Fig. 3F and Table 2). The prominent θ peak observed during baseline persisted during this preLORR period, appearing as a trough ($f_t = 7.2$ Hz) in the difference spectra, and was not significantly different from baseline. At LORR, slow and δ power showed a further significant increase ($f_p = 3.4$ Hz). At higher frequencies, the power shifted toward the α band, but with a peak still within the boundaries of the β band ($f_p = 16.4$ Hz; Fig. 3F and Table 2). The power in the θ band was not significantly different from baseline ($f_t = 6.49$ Hz). After LOM the trend further continued, with an increase in slow and δ power ($f_p = 1.6$ Hz) and a complete shift from the β to the α band ($f_p = 10.6$ Hz). Power in the θ band became significantly higher than baseline ($f_t = 6.5$ Hz) (Fig. 3F and Table 2).

The sequence of electrophysiological changes observed in thalamus during emergence from anesthesia differed from the changes observed during induction, much as we observed in the prelimbic cortex. During PreROM there was a period with evident slow, δ , and α - β power (Fig. 3 G and H), shown in the raw trace (Fig. 3 I) and in the group spectra computed 3 min pre-ROM (δ , $f_p = 2.1$ Hz; α , $f_p = 11$ Hz). At this time, power in the θ band remained not significantly different from baseline (Fig. 3J and Table 2). Immediately after ROM, α power decreased significantly, and the peak shifted to the β band ($f_p = 23.8$ Hz). In addition, slow oscillation power also decreased significantly, approaching baseline levels, whereas a significant δ band peak persisted ($f_p = 3.8$ Hz). θ power significantly decreased relative to baseline ($f_t = 6.6$ Hz) (Table 2). The difference spectrum observed immediately after RORR was very similar to that observed during ROM (Fig. 3I).

Higher-order thalamic nuclei, such as the mediodorsal, central lateral, and sensory-motor (posterior group and laterodorsal) nuclei, have distinct patterns of connectivity with prelimbic

cortex and other subcortical structures (Fig. S3). We therefore characterized oscillations within these different thalamic divisions during induction and emergence. We assigned recording locations to mediodorsal (M: $n = 4$, four rats), central lateral (C: $n = 7$, seven rats), and sensory-motor (S: $n = 17$, seven rats) nuclei (Materials and Methods). During induction of anesthesia, the raw traces recorded during LORR did not display differences in amplitude (Fig. S4). However, the difference spectra revealed that θ power was significantly lower in the sensory-motor nucleus than in the mediodorsal nucleus at LORR ($f_t = 8$ Hz) and at LOM ($f_t = 6.9$ Hz) (Fig. S4). During emergence, the simultaneously recorded LFPs in the different thalamic nuclei did not show visible differences in amplitude (Fig. S4), and accordingly, the spectral analysis showed no differences in power during any of the behavioral events in any of the frequency bands (Fig. S4).

Thalamocortical Synchronization in the α and δ Ranges During Propofol-Induced Anesthesia. Mathematical modeling of propofol-induced dynamics predicts that α oscillations within thalamus and cortex become coherent with increasing potentiation of GABAergic inhibition (14). However, empirical data and analyses to evaluate this hypothesis have been lacking. The role of the thalamus in generating slow and δ oscillations observed during nonrapid eye movement sleep and some states of anesthesia-induced altered consciousness has been a topic of much debate (21). Recordings in deafferented cortex show that slow oscillations can occur in the absence of thalamic connections (22). Yet basic functional anatomic and neurophysiological reasoning suggests that the thalamus is likely a significant participant in slow and δ oscillations (23, 24). To address these questions in the context of induction and emergence from propofol anesthesia, we analyzed the coherence between the superficial layer (2/3, referred to as SL) and deep layers (5 and 6, referred to as DLs), layers of prelimbic cortex, and the different high-order thalamic nuclei (M, C, and S).

In total, we analyzed six thalamocortical combinations, denoted as follows: SL-M ($n = 6$, three rats), DL-M ($n = 7$, three rats), SL-C ($n = 7$, four rats), DL-C ($n = 15$, five rats), SL-S ($n = 16$, four rats), and DL-S ($n = 41$, five rats). The full results of the coherence calculations can be seen in Fig. S5 and are schematized in Fig. 4 and Fig. S6. During the preLORR period, when

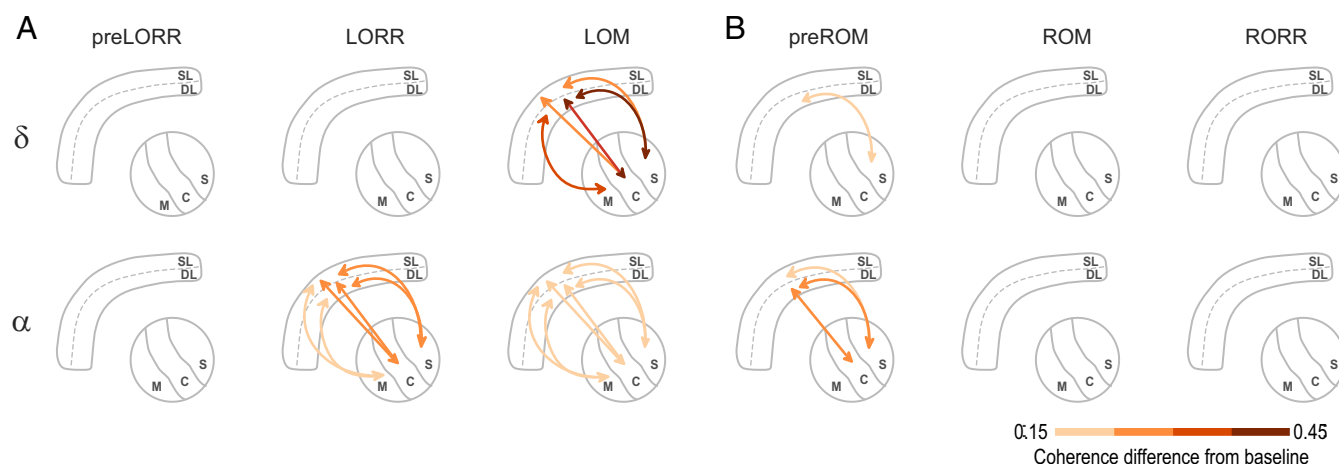


Fig. 4. Changes in thalamocortical coherence with respect to baseline in the δ and α bands. (A and B) Strength of synchronization between deep layers (DL) or superficial layers (SL) of prefrontal cortex and the mediodorsal (M), central lateral (C), and sensory-motor (S) nuclei, within two frequency bands (δ and α , rows) and the three different behavioral states (columns) observed during induction (A) and emergence (B). The arrows depict the establishment of significant changes in coherence between cortical and thalamic nuclei with respect to baseline. The color of the arrows exemplifies the size of the increase (red shades) in coherence.

Thalamocortical Synchronization Dissipates in an Anatomically Discrete Fashion During Emergence from Propofol-Induced Anesthesia.

During emergence, the different thalamocortical pairs displayed different coherence patterns through the different behavioral events. At preROM, the significant δ -band coherence disappeared across most thalamocortical pairs, remaining significantly different from baseline only between the DL-S pair ($f_p = 4.1$ Hz) (Fig. 4B; Fig. S5, fourth row; and Table S2). In the α band, a significant coherence difference in the preROM period remained present between DL-C ($f_p = 12.1$ Hz), SL-S ($f_p = 11.8$ Hz), and DL-S pairs ($f_p = 12.1$ Hz), but there were not significant differences between any of the other pairs. At ROM and RORR, the increase in coherence in δ and α bands disappeared in all pairs (Fig. 4B; Fig. S5, fifth and sixth rows; and Table S2) although we observed a small but significant increase in coherence in the β band at RORR (Figs. S5, sixth row, and S6). Thus, during emergence, thalamocortical coherence dissipated in a graded sequence that did not mirror the onset of coherence during induction, with the S-cortical α coherence being the last to disappear.

Discussion

We observed changes in cortical and thalamic dynamics associated with behavior during gradual induction of and emergence from propofol-induced unconsciousness in rodents. During induction, cortical oscillations followed a pattern that appears similar to that observed in the human scalp EEG, characterized by broad-band β oscillations that coalesce into α oscillations after loss of consciousness (LORR and LOM), paired with the appearance of slow- δ oscillations (LOM). Propofol-induced thalamic oscillations also showed changes associated with different behavioral states, but with less distinct, more broad-band oscillations. Thalamic and cortical oscillations, however, showed significant increases in coherence in the α band at loss of consciousness (LORR) and in the δ band at LOM. This observation is consistent with previous computational modeling studies (14) and invasive recordings in rodents (25). In particular, whereas cortical inhibitory networks can generate β oscillations (26) that slow to α frequencies with increasing inhibitory tone (13), propofol-induced α oscillations appear to become coherent through the functional influence of the thalamus (14). We must emphasize, however, that the presence of thalamocortical coherence implies only an interaction between the two areas, and can-

not convey directional influences, which would require the application of different analysis methods that can be challenging to interpret (27).

During emergence, these propofol-induced dynamics dissipated, but with a trajectory that differed from that observed during induction. In the cortex, we observed an abrupt transition from a slow- δ - α pattern to β oscillations during emergence, distinct from the gradual transition observed during induction. In the thalamus, we observed a similar abrupt transition from slow- δ and broad-band α and β oscillations to just β oscillations, again distinct from the gradual change during induction. Changes in thalamocortical coherence also showed a different trajectory during emergence compared with induction. Whereas during induction, α and δ coherence appeared abruptly at LORR and LOM, respectively, these coherent oscillations dissipated with a distinct sequence across midline and intralaminar, followed by sensory-motor divisions of thalamus. These events may constitute a thalamocortical “boot-up” sequence that occurs during emergence from anesthesia-induced unconsciousness. This dynamic boot-up sequence is consistent with changes in functional connectivity spanning thalamus and prefrontal cortex observed in humans, using positron emission tomography (28) and functional magnetic resonance imaging (15) during emergence from anesthesia. In addition, the asymmetry in cortical, thalamic, and thalamocortical dynamics during induction and emergence appears consistent with previous reports of hysteresis in anesthetic concentrations associated with loss and recovery of consciousness (29).

We designed these studies to characterize thalamocortical dynamics in frontal cortical and higher-order thalamus that have been implicated as key sites of action in modeling studies (14) and in previous studies of propofol in humans (15). The rodent prefrontal cortex is a component of the rodent medial prefrontal cortex, which is homologous to the human medial prefrontal cortex (30). The mediodorsal, central lateral, posterior medial, and laterodorsal thalamic nuclei, which respectively are part of the midline, intralaminar, and multimodal higher-order thalamic divisions, also have homologs in humans. These nuclei are regarded as higher-order thalamic nuclei, defined by the fact that they receive inputs primarily from cortical layer 5, compared with first-order nuclei, which receive input primarily from ascending sensory pathways (31). The higher-order nuclei are thus thought to influence high-order cortical functions: They constitute a substantial portion of the thalamic “matrix” and are also categorized

as part of the “nonspecific” thalamus. The medial prefrontal cortex has highly structured interconnections with these higher-order nuclei, as indicated in Fig. S3. Our findings are thus consistent with functional magnetic resonance imaging studies in humans that describe reductions in functional connectivity between nonspecific thalamus and frontal cortex during propofol-induced sedation (15).

Our finding that propofol-induced oscillations have greater power in the deep layers of prefrontal cortex (Fig. 2) is consistent with a disruption of not only cortical activity, but also cortico-thalamic activity, because cortico-thalamic projections originate from the deep layers (Fig. S3). At the same time, the significant involvement of superficial cortical layers in the propofol-induced oscillations (Fig. 4) suggests that cortico-cortical connections could be disrupted as well, because cortico-cortical connections originate and terminate within the superficial layers. The coherent oscillations we observed in the α band at LORR and LOM in cortex and thalamus are consistent with the thalamocortical mechanism proposed in Ching et al. (14). Our studies add the observation that at LOM, cortical and thalamic oscillations are coherent at δ frequencies also. This progression from α coherence at LORR to α plus δ coherence at LOM is consistent with a thalamic mechanism in which the thalamus becomes increasingly hyperpolarized (32) at increasing levels of propofol administration, first in a way that promotes coherent α oscillations and then in a way that facilitates both coherent δ and α oscillations (33). The observation that δ oscillations become coherent at loss of movement could be useful clinically as an indicator of akinesia, particularly if noninvasive measures of this phenomenon could be developed.

During emergence, we observed changes in oscillatory activity and thalamocortical coherence that differed from induction in specific components of prefrontal cortex and thalamus. We observed that α coherence between superficial cortical layers and midline and intralaminar thalamic nuclei appeared to recover before recovery of movement (preROM; Fig. 4B), again consistent with a “boot-up sequence” during emergence distinct from induction. If this reflects a recovery of function within the superficial cortical layers, it might also imply that cortico-cortical functional connectivity has been restored, at least in part, in this state. Given the structure of cortico-thalamic projections (Fig. S3), the recovery of the superficial layers at preROM also suggests that the remaining α and δ coherence with intralaminar and sensory-motor thalamus most likely originates from the deep cortical layers. ROM is associated with loss of the remaining coherence between prefrontal cortex and intralaminar and sensory-motor thalamic nuclei. Sensory-motor thalamus engages broadly with both somatosensory and motor cortex, as well as other cortical regions, providing a means of coordination between these areas. The recovery of coherence between sensory-motor thalamus and prefrontal cortex suggests that recovery of executive functions mediated by medial prefrontal cortex and midline/intralaminar thalamus on the one hand and integration of somatosensory, motor, and other functions in the other (34) could be prerequisites for recovery of movement.

This boot-up sequence would be consistent with a mechanism in which ascending arousal inputs from cholinergic and dopaminergic centers actively drive recovery of circuit function. Cholinergic projections from basal forebrain show a preference for mediodorsal and intralaminar thalamic nuclei (31, 35–38). Dopaminergic projections from the ventral tegmental area in the rat target primarily the reticular nucleus, zona incerta, and mediodorsal nucleus (39). In addition, in primates, projections from the ventral tegmental area (VTA) to the mediodorsal nucleus lack the dopamine transporter, thus potentiating dopaminergic signaling in this nucleus (40). VTA projections to the cortex induce superficial layer cortical postsynaptic depolarizations (41), which is consistent with the loss of coherence

we observed in superficial layers of cortex at preROM. A number of other investigations have reported cholinergic (42–44) and dopaminergic (45, 46) influences on arousal that provoke recovery of consciousness after anesthesia-induced unconsciousness. Our work, alongside this evidence from previous studies, suggests that the “hysteresis” during emergence from anesthesia-induced unconsciousness (29) could be explained by active enhancement of arousal from the basal forebrain and VTA.

In both rodents and humans, the medial prefrontal cortex is part of a larger resting-state “default mode” network that is active in the absence of external stimuli and that is functionally connected with thalamus (47). The medial prefrontal cortex in particular is active in self-referential tasks (48) and during states of “internal consciousness” (49). The mediodorsal thalamus is the primary relay nucleus for the medial prefrontal cortex. Our finding that medial prefrontal cortex and mediodorsal thalamus are both engaged in narrow, highly coherent oscillations suggests that processing within these structures would be impaired, including functions related to self-reference or internal consciousness. Thus, our findings imply that when these propofol-induced oscillations appear at LORR/LOM, they are indicative of a state of impaired self-awareness and impaired internal consciousness. At the same time, during emergence, our results show that there is a period before ROM (preROM) where these oscillations dissipate and activity within this medial prefrontal and mediodorsal thalamic circuit is restored, at least in part. At the same time α coherence between sensory-motor thalamic and prefrontal cortex persists, dissipating only at ROM. This suggests that, in this preROM state, cortical and thalamic functions associated with self-awareness and internal consciousness could be restored as part of the boot-up sequence, despite ongoing impairment of sensory-motor function.

The propofol-induced oscillations we observed in the rodent prefrontal cortex are similar in character to those that are routinely observed in the scalp EEG in humans, despite notable interspecies differences in cortical and thalamic architecture. Rodent prefrontal cortex is agranular; i.e., it does not present a layer 4 (50). In primates the prefrontal cortex is granular, suggesting that layer 4 is not required to produce these oscillations. Inhibitory interneurons are absent in rodent dorsal thalamus, but are present in primate dorsal thalamus (51). This suggests, consistent with previous computational modeling studies (14), that inhibition from ventral structures such as the thalamic reticular nucleus, which are common to both primates and rodents, is likely responsible for the changes in thalamocortical coherence observed under propofol.

Thalamic and cortical recordings have been performed previously during propofol-induced unconsciousness in rodents (25). Our studies add significantly to these previous studies by characterizing frequency-dependent functional relationships (coherence) between thalamus and cortex, analyzing dynamics in these structures during a gradual induction and during emergence, analyzing the interactions between different thalamic divisions and prefrontal cortex lamina throughout induction and emergence, and characterizing propofol-induced changes in slow and δ oscillations. The gradual infusion scheme, in combination with a more detailed behavioral analysis, allowed us to identify distinct dynamics for LORR and LOM during induction and preROM, ROM, and RORR during emergence. As discussed here, the distinct thalamocortical dynamics during these states have important implications for understanding the functional mechanisms underlying propofol-induced loss and recovery of consciousness.

Previous studies in humans have observed significant increases in slow oscillation power during loss of consciousness (7, 12) and have established that these oscillations correspond to ON and OFF states where neurons are periodically silenced (11). Notably, unlike propofol-induced α waves, these slow oscillations

are spatially incoherent (7, 11), implying a state of “fragmentation” of cortical activity (11). Our results are consistent with these previous findings, as slow oscillation power increases significantly at LORR and LOM in both prefrontal cortex and thalamus and dissipates before ROM. Our results also point to functional distinctions between slow and δ oscillations: Whereas slow oscillations appear to be incoherent across cortex (7, 11), and between cortex and thalamus (Fig. S6), δ oscillations are coherent between cortex and thalamus. This suggests that slow oscillations might be generated locally in different regions of cortex or thalamus (22, 24, 52, 53), whereas δ oscillations involve interactions between cortex and thalamus (54, 55). Overall, our results suggest that propofol can induce a variety of dynamics that mediate functional impairment of both cortical and thalamocortical circuits.

We also observed important changes in θ power in thalamic oscillations and thalamocortical coherence. The θ oscillations in the thalamus disappeared during induction of anesthesia, consistent with its relationship to arousal, but paradoxically, θ power remained lower than baseline after emergence from anesthesia (Fig. 3). Similar results have been found in our laboratory during active emergence from propofol induced by methylphenidate in rodents (45), suggesting that the animals are in a state of arousal that is different from the normal awake state. In the present study we did not have a specific hypothesis to test regarding changes in thalamocortical θ coherence. It is still debated whether θ oscillations recorded in the thalamus are locally generated (56) or generated by primary currents within hippocampus. Propofol and other GABAergic anesthetic drugs are known to impair memory, even after recovery of consciousness (57). We speculate that this sustained reduction in θ power after RORR could reflect ongoing memory impairment.

We performed recordings from a single cortical area, prelimbic cortex. This decision was informed by the previous modeling studies of α oscillations (14). Future studies could record from multiple cortical areas to characterize whether they participate in these dynamics. The anterior cingulate is part of the rodent medial prefrontal cortex, directly adjacent to the prelimbic cortex, and has a similar pattern of thalamic structural connections. The anterior cingulate is involved in salience processing, which we predict would be impaired during anesthesia-induced sedation and unconsciousness. The posterior cingulate, part of the default mode network, would be another area of interest. Recordings from anterior and posterior cingulate cortices could help characterize the extent to which anterior–posterior functional interactions are disrupted by anesthetic drugs to produce unconsciousness. These studies could also help elucidate the role of frontal cortex in the generation of the propofol-induced α rhythm, which in human scalp EEG is seen predominantly on frontal electrodes (7). Our analysis pooled recordings from layers 5 and 6 to maximize the data available to estimate coherence with different thalamic nuclei. Future studies could focus separately on layers 5 and 6, to characterize how their distinct “driver” and “modulator” functions, respectively, change during different states of anesthesia-induced altered arousal.

Our studies provide in vivo evidence for the role of thalamocortical synchronization as a mechanism for propofol-induced

unconsciousness, first proposed by Ching et al. (14). In addition, our work characterizes in detail thalamocortical dynamics during emergence, establishing a pattern of functional recovery that is consistent with a mechanism of active arousal from dopaminergic and cholinergic centers and that may underlie previous reports of hysteresis in anesthetic induction and emergence. Together with previous studies of propofol-induced slow oscillations, this work suggests that propofol can induce a variety of dynamics that mediate functional impairment of both cortical and thalamocortical circuits during altered arousal and unconsciousness. The homologous relationships between rodent and human medial prefrontal cortex and thalamus imply that when these oscillatory dynamics are present, self-awareness and internal consciousness would be impaired or abolished. These studies therefore significantly advance our understanding of what it means to be unconscious under anesthesia and further establish dynamic neurophysiological markers that can define when we truly are.

Materials and Methods

Surgery and Animal Care. We conducted all animal work in accordance with federal, state, and local regulations and following NIH guidelines and standards. The corresponding protocols 0511-044-14 and 0511-038-17 were approved by the Institutional Animal Care and Use Committee (IACUC) at the Massachusetts Institute of Technology (*SI Materials and Methods*).

Anesthetic Protocol, Data Acquisition, and Spectral Analysis. We performed the propofol infusion through an i.v. cannula inserted in the tail vein. We infused propofol at a constant rate of $1.67 \text{ mg} \cdot \text{kg}^{-1} \cdot \text{min}^{-1}$. We tested for loss of consciousness, using the LORR assay. Rats were left in the supine position until RORR. We used video recordings for posterior identification of the latency to pica and to obtain the latency to LOM and to ROM. LFPs were recorded for about 15 min before the start of infusion and up to 1 hour after the RORR. Raw data can be found in *Datasets S1–S5*. Electrodes with poor signal quality and movement artifacts were visually rejected by two experienced researchers (F.J.F. and K.E.H.) based on spectral and time-domain characteristics. Spectrograms were computed with the multitaper method (18) (Code available at Chronux). To assess statistical significance for the difference in spectra at each frequency, we computed the 99% confidence intervals by using a published bootstrap algorithm (58, 59). Only the frequencies whose confidence intervals did not include zero within at least one complete bandwidth unit (3 Hz for spectra and 1.5 Hz for coherence) were considered to be statistically significant (*SI Materials and Methods*). All analysis were performed in MATLAB.

Histology. After completing the experiment, we stained brain slices using the Nissl method. We identified the frontal cortical layers based on the size, density, and distribution of neuronal somata (*SI Materials and Methods*). We identified thalamic nuclei and subregions by coregistration with a stereotaxic atlas (60) (*SI Materials and Methods*). We pooled the electrodes located in the laterodorsal nucleus ventrolateral and dorsomedial parts and in the posterior thalamic group within the S denomination. The other electrodes were identified as located in the M central and lateral nuclei and in the C nucleus. Electrodes found to be in other locations were not included in the analysis.

ACKNOWLEDGMENTS. The authors are grateful to Carmen Varela and Maria Jose Galazo for numerous conversations and suggestions. This work was supported by National Institutes of Health Grants DP2OD006454 (to P.L.P.), TR01GM104948 (to E.N.B. and M.A.W.), and P01GM118269 (to E.N.B.).

- Brown EN, Lydic R, Schiff ND (2010) General anesthesia, sleep, and coma. *N Engl J Med* 363:2638–2650.
- Rudolph U, Antkowiak B (2004) Molecular and neuronal substrates for general anaesthetics. *Nat Rev Neurosci* 5:709–720.
- Alkire MT, Hudetz AG, Tononi G (2008) Consciousness and anesthesia. *Science* 322:876–880.
- Franks NP (2008) General anaesthesia: From molecular targets to neuronal pathways of sleep and arousal. *Nat Rev Neurosci* 9:370–386.
- Brown EN, Purdon PL, Van Dort CJ (2011) General anesthesia and altered states of arousal: A systems neuroscience analysis. *Annu Rev Neurosci* 34:601–628.
- Concas A, et al. (1990) The general anesthetic propofol enhances the function of gamma-aminobutyric acid-coupled chloride channel in the rat cerebral cortex. *J Neurochem* 55:2135–2138.
- Purdon PL, et al. (2013) Electroencephalogram signatures of loss and recovery of consciousness from propofol. *Proc Natl Acad Sci USA* 110:E1142–E1151.
- Feshchenko VA, Veselis RA, Reinsel RA (2004) Propofol-induced alpha rhythm. *Neuropsychobiology* 50:257–266.
- Supp GG, Siegel M, Hipp JF, Engel AK (2011) Cortical hypersynchrony predicts breakdown of sensory processing during loss of consciousness. *Curr Biol* 21:1988–1993.
- Cimens A, et al. (2011) Tracking brain states under general anesthesia by using global coherence analysis. *Proc Natl Acad Sci USA* 108:8832–8837.

11. Lewis LD, et al. (2012) Rapid fragmentation of neuronal networks at the onset of propofol-induced unconsciousness. *Proc Natl Acad Sci USA* 109:E3377–E3386.
12. Ni Mhuircheartaigh R, Warnaby C, Rogers R, Jbabdi S, Tracey I (2013) Slow-wave activity saturation and thalamocortical isolation during propofol anesthesia in humans. *Sci Transl Med* 5:208ra148.
13. McCarthy MM, Brown EN, Kopell N (2008) Potential network mechanisms mediating electroencephalographic beta rhythm changes during propofol-induced paradoxical excitation. *J Neurosci* 28:13488–13504.
14. Ching SN, Cimenser A, Purdon PL, Brown EN, Kopell NJ (2010) Thalamocortical model for a propofol-induced alpha-rhythm associated with loss of consciousness. *Proc Natl Acad Sci USA* 107:22665–22670.
15. Liu X, Lauer KK, Ward BD, Li S-J, Hudetz AG (2013) Differential effects of deep sedation with propofol on the specific and nonspecific thalamocortical systems: A functional magnetic resonance imaging study. *Anesthesiology* 118:59–69.
16. Mukamel EA, et al. (2014) A transition in brain state during propofol-induced unconsciousness. *J Neurosci* 34:839–845.
17. Vertes RP (2002) Analysis of projections from the medial prefrontal cortex to the thalamus in the rat, with emphasis on nucleus reuniens. *J Comp Neurol* 442:163–187.
18. Mitra P, Bokil H (2007) *Observed Brain Dynamics* (Oxford Univ Press, New York).
19. Freeman WJ, Rogers LJ, Holmes MD, Silbergeld DL (2000) Spatial spectral analysis of human electrocorticograms including the alpha and gamma bands. *J Neurosci Methods* 95:111–121.
20. Buzsáki G (2002) Theta oscillations in the hippocampus. *Neuron* 33:325–340.
21. Crunelli V, David F, Lörincz ML, Hughes SW (2015) The thalamocortical network as a single slow wave-generating unit. *Curr Opin Neurobiol* 31:72–80.
22. Timofeev I, Steriade M (1996) Low-frequency rhythms in the thalamus of intact-cortex and decorticated cats. *J Neurophysiol* 76:4152–4168.
23. David F, et al. (2013) Essential thalamic contribution to slow waves of natural sleep. *J Neurosci* 33:19599–19610.
24. Lewis LD, et al. (2015) Thalamic reticular nucleus induces fast and local modulation of arousal state. *Elife* 4:e08760.
25. Baker R, et al. (2014) Altered activity in the central medial thalamus precedes changes in the neocortex during transitions into both sleep and propofol anesthesia. *J Neurosci* 34:13326–13335.
26. Le Van Quyen M, et al. (2016) High-frequency oscillations in human and monkey neocortex during the wake–sleep cycle. *Proc Natl Acad Sci USA* 113:9363–9368.
27. Stokes PA, Purdon PL (2017) Study of problems encountered in Granger causality analysis from a neuroscience perspective. *Proc Natl Acad Sci USA*, 10.1073/pnas.1704663114.
28. Långsjö JW, et al. (2012) Returning from oblivion: Imaging the neural core of consciousness. *J Neurosci* 32:4935–4943.
29. Friedman EB, et al. (2010) A conserved behavioral state barrier impedes transitions between anesthetic-induced unconsciousness and wakefulness: Evidence for neural inertia. *PLoS One* 5:e11903.
30. Hoover WB, Vertes RP (2007) Anatomical analysis of afferent projections to the medial prefrontal cortex in the rat. *Brain Struct Funct* 212:149–179.
31. Varela C (2014) Thalamic neuromodulation and its implications for executive networks. *Front Neural Circuits* 8:69.
32. Alkire MT, Haier RJ, Fallon JH (2000) Toward a unified theory of narcosis: Brain imaging evidence for a thalamocortical switch as the neurophysiologic basis of anesthetic-induced unconsciousness. *Conscious Cognit* 9:370–386.
33. Hughes SW, Crunelli V (2005) Thalamic mechanisms of EEG alpha rhythms and their pathological implications. *Neuroscientist* 11:357–372.
34. Nosedá R, Jakubowski M, Kainz V, Borsook D, Burstein R (2011) Cortical projections of functionally identified thalamic trigeminovascular neurons: Implications for migraine headache and its associated symptoms. *J Neurosci* 31:14204–14217.
35. Parent A, Paré D, Smith Y, Steriade M (1988) Basal forebrain cholinergic and non-cholinergic projections to the thalamus and brainstem in cats and monkeys. *J Comp Neurol* 277:281–301.
36. Hallanger AE, Price SD, Lee HJ, Steininger TL, Wainer BH (1990) Ultrastructure of cholinergic synaptic terminals in the thalamic anteroventral, ventroposterior, and dorsal lateral geniculate nuclei of the rat. *J Comp Neurol* 299:482–492.
37. Heckers S, Geula C, Mesulam MM (1992) Cholinergic innervation of the human thalamus: Dual origin and differential nuclear distribution. *J Comp Neurol* 325:68–82.
38. Gritti I, Mariotti M, Mancia M (1998) GABAergic and cholinergic basal forebrain and preoptic anterior hypothalamic projections to the mediodorsal nucleus of the thalamus in the cat. *Neuroscience* 85:149–178.
39. García-Cabezas MA, Martínez-Sánchez P, Sánchez-González MA, Garzon M, Cavada C (2009) Dopamine innervation in the thalamus: Monkey versus rat. *Cereb Cortex* 19:424–434.
40. García-Cabezas MA, Rico B, Cavada C (2005) The primate thalamus is a key target for brain dopamine. *J Neurosci* 25:6076–6083.
41. Iwashita M (2014) Phasic activation of ventral tegmental neurons increases response and pattern similarity in prefrontal cortex neurons. *Elife* 3:e02726.
42. Alkire MT, McReynolds JR, Hahn EL, Trivedi AN (2007) Thalamic microinjection of nicotine reverses sevoflurane-induced loss of righting reflex in the rat. *Anesthesiology* 107:264–272.
43. Pal D, Silverstein BH, Lee H, Mashour GA (2016) Neural correlates of wakefulness, sleep, and general anesthesia: An experimental study in rat. *Anesthesiology* 125: 929–942.
44. Meuret P, Backman SB, Bonhomme V, Plourde G, Fiset P (2000) Physostigmine reverses propofol-induced unconsciousness and attenuation of the auditory steady state response and bispectral index in human volunteers. *Anesthesiology* 93:708–717.
45. Chemali JJ, Van Dort CJ, Brown EN, Solt K (2012) Active emergence from propofol general anesthesia is induced by methylphenidate. *Anesthesiology* 116:998–1005.
46. Solt K, et al. (2011) Methylphenidate actively induces emergence from general anesthesia. *Anesthesiology* 115:791–803.
47. Akeju O, et al. (2014) Disruption of thalamic functional connectivity is a neural correlate of dexmedetomidine-induced unconsciousness. *Elife* 3:e04499.
48. Gusnard DA, Akbudak E, Shulman GL, Raichle ME (2001) Medial prefrontal cortex and self-referential mental activity: Relation to a default mode of brain function. *Proc Natl Acad Sci USA* 98:4259–4264.
49. Vanhaudenhuyse A, et al. (2011) Two distinct neuronal networks mediate the awareness of environment and of self. *J Cogn Neurosci* 23:570–578.
50. Ongür D, Price JL (2000) The organization of networks within the orbital and medial prefrontal cortex of rats, monkeys and humans. *Cereb Cortex* 10:206–219.
51. Timofeev I, Chauvette S (2011) Thalamocortical oscillations: Local control of EEG slow waves. *Curr Top Med Chem* 11:2457–2471.
52. Nir Y, et al. (2011) Regional slow waves and spindles in human sleep. *Neuron* 70:153–169.
53. Vyazovskiy VV, et al. (2011) Local sleep in awake rats. *Nature* 472:443–447.
54. Hill S, Tononi G (2005) Modeling sleep and wakefulness in the thalamocortical system. *J Neurophysiol* 93:1671–1698.
55. Crunelli V, Hughes SW (2010) The slow (<1 Hz) rhythm of non-REM sleep: A dialogue between three cardinal oscillators. *Nat Neurosci* 13:9–17.
56. Vertes RP, Albo Z, Viana Di Prisco G (2001) Theta-rhythmically firing neurons in the anterior thalamus: Implications for mnemonic functions of Papez's circuit. *Neuroscience* 104:619–625.
57. Veselis RA, et al. (2008) Low-dose propofol-induced amnesia is not due to a failure of encoding: Left inferior prefrontal cortex is still active. *Anesthesiology* 109:213–224.
58. Akeju O, et al. (2016) Electroencephalogram signatures of ketamine anesthesia-induced unconsciousness. *Clin Neurophysiol* 127:2414–2422.
59. Cornelissen L, Kim S-E, Purdon PL, Brown EN, Berde CB (2015) Age-dependent electroencephalogram (EEG) patterns during sevoflurane general anesthesia in infants. *Elife* 4:e06513.
60. Paxinos G, Watson C (2007) *The Rat Brain in Stereotaxic Coordinates* (Elsevier, Amsterdam).
61. Shafer SL, Gregg KM (1992) Algorithms to rapidly achieve and maintain stable drug concentrations at the site of drug effect with a computer-controlled infusion pump. *J Pharmacokinet Biopharm* 20:147–169.
62. Larsson JE, Wahlström G (1994) Optimum rate of administration of propofol for induction of anaesthesia in rats. *Br J Anaesth* 73:692–694.
63. Shyr M-H, Tsai T-H, Tan PPC, Chen C-F, Chan SHH (1995) Concentration and regional distribution of propofol in brain and spinal cord during propofol anesthesia in the rat. *Neurosci Lett* 184:212–215.
64. Reed SJ, Plourde G (2015) Attenuation of high-frequency (50–200 Hz) thalamocortical EEG rhythms by propofol in rats is more pronounced for the thalamus than for the cortex. *PLoS One* 10:e0123287.
65. Kleitman N (1957) Sleep, wakefulness, and consciousness. *Psychol Bull* 54:354–359.
66. Franks NP, Zecharia AY (2011) Sleep and general anesthesia. *Can J Anesth* 58:139–148.
67. Petrenko AB, et al. (2004) Reduced sensitivity to ketamine and pentobarbital in mice lacking the N-Methyl-D-Aspartate receptor GluR1 subunit. *Anesth Analg* 99: 1136–1140.
68. Davis TG (2016) Pica in rats as a preclinical model of emesis. *Curr Protoc Neurosci* 77:9.53.1–9.53.6.

Supporting Information

Flores et al. 10.1073/pnas.1700148114

SI Materials and Methods

Surgery and Animal Care. We used a total of eight Sprague-Dawley rats for all experiments (Charles River). Rats weighed between 400 g and 600 g. The rats were individually caged and kept in a humidity- and temperature-controlled room, under a 12-hour/12-hour light/dark cycle. We performed all experiments during the daytime. We implanted the electrodes under continuous 2% isoflurane anesthesia. We administered buprenorphine (0.01 mg/kg) i.p. for analgesia right before surgery and then every 12 hours for 2 days after surgery. We implanted two silicon probes (Neuronexus Technologies) in each animal, each probe aiming for prefrontal or thalamic regions. Each probe had 32 recording sites, distributed equally in four shanks. In the prefrontal probe (A4x8-5mm-200-177) the distance between shanks was 200 μm . In the thalamic probe (A4x8-5mm-400-177) the distance between shanks was 400 μm . In both probes, the length spanned by the recording sites was 700 μm . We positioned the probes stereotactically, with the prefrontal probe aiming to the left prelimbic area [antero-posterior (AP): +3.0 mm; medio-lateral (ML): -0.1 mm to -1.1 mm; dorso-ventral (DV): +3.2 mm] (Fig. S1A) and the thalamic probe aiming to left midline, intralaminar, and sensory nuclei (AP: -3.0; ML: -0.8 to -1.8; DV: +5.0) (Fig. S1B).

Anesthetic Protocol, Data Acquisition, and Spectral Analysis. Seven days after surgery, we placed the animals in a cylindrical recording chamber (35 cm diameter \times 34 cm height). We performed the propofol infusion through a 24-gauge intravenous cannula inserted in the tail vein. We infused propofol using a Physio 22 syringe pump (Harvard Apparatus), controlled through STANPUMP (61) running on Windows XP 32-bit (Microsoft). Constant rate infusion (CRI) of propofol was performed for 15 min at a rate of $1.67 \text{ mg} \cdot \text{kg}^{-1} \cdot \text{min}^{-1}$, for a total dose of 25 mg/kg. We used commercially available propofol (10 mg/mL; Hospira) in all experiments. We chose this rate to ensure that all of the rats would lose the righting reflex, based on published studies (62–64), pilot infusions, and simulations with STANPUMP. One of the rats underwent the CRI protocol three times, whereas another two rats underwent the protocol twice. We treated these replicates independently because they were performed at least 11 days apart. For the rat that underwent the protocol three times, the recording quality was very poor for the third replicate; we therefore discarded the data from this third replicate. In summary, we analyzed a total of 11 experiments.

LFPs were recorded for 15 min before the start of infusion and up to 1 hour after RORR. During acquisition, signals were filtered between 0.1 Hz and 500 Hz and referenced to a local reference site in each probe, located at 1.7 mm from the tip of the probe. The signals were acquired at 2,713 Hz, using a Digital-Lynx system and Cheetah recording software (Neuralynx), and downsampled 10 times before analysis. Electrodes with poor signal quality and movement artifacts were visually rejected by two experienced researchers (F.J.F. and K.E.H.), based on spectral and time-domain characteristics, and confirmed by automated movement analysis of the recorded videos. Spectrograms were computed using the multitaper method, with window lengths of 2 s and 1 s of overlap, a time-bandwidth product $TW = 3$, and number of tapers $K = 5$, resulting in a spectral resolution of 3 Hz. To compute spectra and coherence, 1 min of signal was extracted around a behavioral event and divided in nonoverlapping segments of 4 s, with a time-bandwidth product $TW = 3$, and number of tapers $K = 5$, resulting in a spectral resolution of 1.5 Hz.

All spectral analysis was carried out using the Chronux toolbox (18).

To assess statistical significance for the difference in spectra at each frequency, we computed the 99% confidence intervals by randomly drawing spectra with replacement from spectrograms over all time windows, to generate the bootstrapped spectrogram. We took the median from the bootstrapped spectrogram over time for each subject. We calculated differences between two median spectra across different states or layers for each subject and took a median difference across subjects. We repeated this procedure 10,000 times and calculated the 99% confidence interval of the median difference at each frequency. Only the frequencies whose confidence intervals did not include zero within at least one complete bandwidth unit (3 Hz for spectra and 1.5 Hz for coherence) were considered to be statistically significant (58, 59).

Behavioral Testing and Analysis. We tested for loss of consciousness, using the LORR assay, a common measure of loss of consciousness for rodents (65, 66). We assessed the latency to LORR by quickly placing the rat in the supine position every minute. Complete LORR was declared if the rat was not able to return to normal standing position within 30 s (67). Rats were left in the supine position until RORR. In all experiments, we continuously monitored and recorded behavior with a zenithal video camera. We used these video recordings for posterior identification of the latency to pica, defined as the first time point when the rats start chewing the paper in the floor of the cage, after the start of propofol infusion. We also used the video recording to obtain the latency to LOM and to ROM by offline observation of the videos obtained during the experiments. LOM was defined as the first time point after LORR that was followed by complete absence of movement for at least 5 min. Recovery of movement was defined as the first time point after LOM when movement was observed. Statistical analysis of behavioral event latencies was performed using MATLAB (The Mathworks).

Histology. After experiment completion, we deeply anesthetized the rats with isoflurane (2%) and made electrolytic lesions by passing a 5- μA current for 2 s. We then euthanized the rats with a lethal dose of FatalPlus (200 mg/kg) and perfused them with ice-cold 10% formalin. We extracted the brains, kept them in 10% formalin for 2–3 days, and then subsequently sliced them using a VT1000S vibratome (Leica Biosystems). We stained the slices using the Nissl method and imaged them at $2.5\times$, using a bright-field microscope with an automated stage (Carl Zeiss Microscopy) (Fig. S1A and B). We constructed the photomontages using Zen Blue software (Carl Zeiss Microscopy) and adjusted for brightness and contrast, using Adobe Photoshop CC.

We identified the frontal cortical layers based on the size, density, and distribution of neuronal somata. Layer 1 is the most superficial layer and contains almost no cells. Layer 2/3 has a greater cell density than the other layers, with cells that are slightly smaller than the pyramidal cells found in layer 5. The pyramidal cells in layer 5 are larger and have a distribution that is less structured than those in the other layers. The neurons in layer 6 have a smaller diameter than those in layer 5 and are organized in a row-like array within the layer (Fig. S1C). We identified thalamic nuclei and subregions by coregistration with a stereotaxic atlas (60), using the internal capsule and the dorsal third ventricle as landmarks. We pooled

the electrodes located in the laterodorsal nucleus ventrolateral and dorsomedial parts and in the posterior thalamic group within the sensory-motor denomination. The other electrodes were identified as located in the central and lateral mediodorsal nuclei and in the central lateral nucleus (Fig. S1D). Electrodes found to be in other locations were not included in the analysis.

SI Results

Temporal Correlations Between Behavioral Events. In all of the experiments, the first behavioral sign we observed was pica, which is defined as the consumption of nonnutritious material (68). Pica was manifested as chewing the paper towel located in the bottom of the recording chamber. Pica started soon after we started the infusion of the drug (median, 2.5 min; range, 4.3 min) (Fig. S2A), and it was consistently followed by a progressive inability to sustain a normal standing position. LORR occurred soon afterward (median, 7.78 min; range, 5.26 min) (Fig. S2A). We investigated the temporal correlation between pica and LORR and found that the linear fit is not significantly different from that of a constant model [$F_{(1,9)} = 0.86$, $P = 0.38$, $R^2 = 0.09$] (Fig. S2B). Also, the 95% confidence intervals (CIs) of the slope estimate include zero (slope: -0.29 , CI = $[-0.99, 0.41]$). These results provide evidence that pica and LORR are temporally uncorrelated.

After LORR, all animals manifested some amount of movement in the paws and head. Therefore, we also identified the time at which complete LOM occurred. The median latency to LOM was 8.63 min (range: 4.82 min) (Fig. S2A). A multiple-

regression model that included both LORR and pica latencies provides evidence for a positive linear relationship between the latency to LORR and the latency to LOM [$F_{(1,8)} = 17.181$, $P = 0.003$, $R^2_{adj} = 0.61$] (Fig. S2C). Also, the slope estimate CIs do not include zero (slope = 0.93 , 95% CI = $[0.41, 1.44]$). Consistent with the observation that LORR and pica were unrelated, pica did not have a significant effect on the latency to LOM within the multiple-regression model [$F_{(1,8)} = 0.42$, $P = 0.54$]. The CI of the slope estimate for pica also included zero (slope = 0.14 , CI = $[-0.36, 0.64]$). Therefore, LORR and LOM show a significant temporal correlation, whereas pica is not temporally related to any of them.

After the end of the infusion, as animals emerged from anesthesia, ROM was observed with a median latency of 12.65 min (range = 12.95 min) (Fig. S2D). ROM always occurred before or at the same time as RORR, with the rats starting to move their heads or paws or even grooming before fully righting themselves. RORR had a median latency of 13.97 min (range = 10.97 min) (Fig. S2D). As we found with the latencies to LORR and LOM, we also found a positive linear relationship between the latency to ROM and the latency to RORR [$F_{(1,9)} = 68.43$, $P \ll 0.001$, $R^2 = 0.88$] (Fig. S2E). The CI of the slope did not include zero (slope = 0.72 , CI = $[0.52, 0.92]$). We did not observe pica after emergence in any of the experiments.

Because pica does not have a significant temporal relationship with LORR and LOM and is not present during emergence, we focused our analyses of the electrophysiological data on the behavioral endpoints most strongly related to LORR and RORR and LOM and ROM.

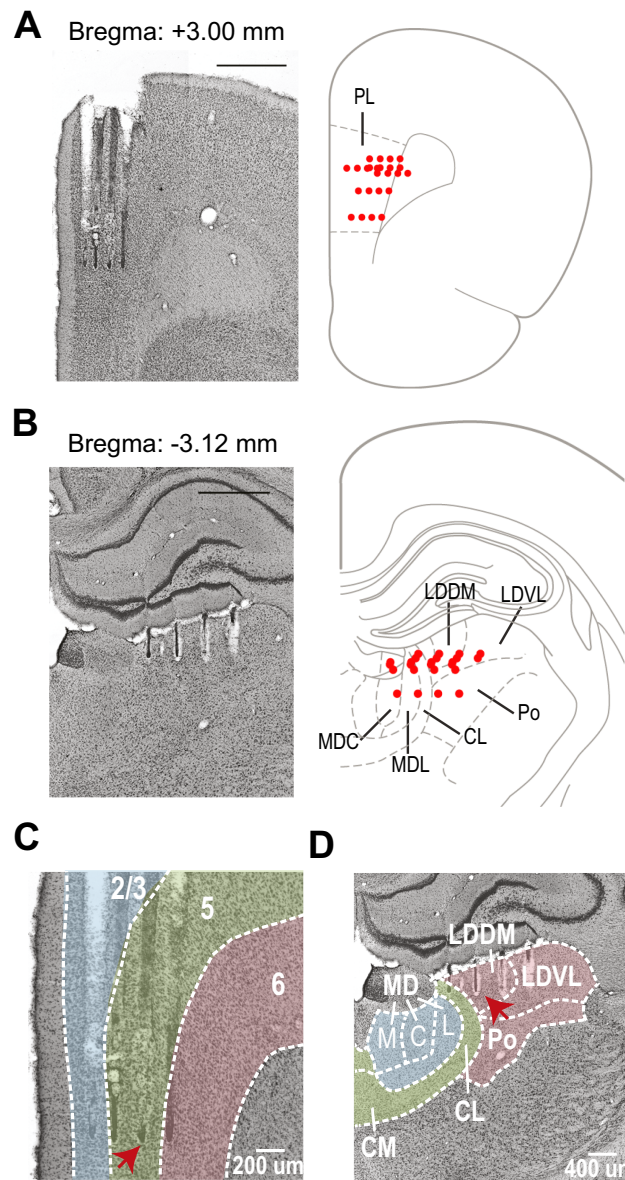


Fig. S1. Histological localization of electrodes targeting prelimbic cortex and higher-order thalamic nuclei. (A, Left) Example of electrode locations in prelimbic cortex (PL) in a coronal slice. The probes left a clear track in the tissue. (A, Right) Summary of prelimbic electrode locations (red circles) across all rats, projected into a coronal slice +3.00 mm anterior to Bregma. (B, Left) Example of electrode locations in the thalamus in a coronal slice. The tracks left by the probes can be easily observed. (B, Right) Summary of thalamic electrode locations across all rats, projected into a coronal slice -3.12 mm from Bregma. (C) Example of assignment of different shanks to different layers of prelimbic cortex. (D) Example of assignment of different shanks to different nuclei of dorsal thalamus. All slices were stained with the Nissl procedure. CL, central lateral thalamic nucleus; LDDM, laterodorsal thalamic nucleus, dorsomedial part; LDVL, laterodorsal thalamic nucleus, ventrolateral part; MDC, mediodorsal thalamic nucleus, central part; MDL, mediodorsal thalamic nucleus, lateral part; MDM, mediodorsal thalamic nucleus, medial part; Po, posterior thalamic nuclear group.

Fig. S3. Schema of anatomical thalamocortical connections.

Fig. S5. Thalamocortical coherence difference with baseline across all behavioral states. In this plot matrix, the rows correspond to the different combinations of SLs and DLs and M, C, and S thalamic nuclei. The columns correspond the different behavioral states (main text). The coherence difference is a dimensional.

